Letter

ADVANCED PHOTONICS

Enhanced generation of nondegenerate photon pairs in nonlinear metasurfaces

Matthew Parry,[a,b,*] Andrea Mazzanti,[a,c] Alexander Poddubny,[a,d,e] Giuseppe Della Valle,[c,f] Dragomir N. Neshev,[a,b] and Andrey A. Sukhorukov[a,b,*]

[a]Australia National University, Research School of Physics, Canberra, Australia
[b]ARC Centre of Excellence for Transformative Meta-Optical Systems, Canberra, Australia
[c]Politecnico di Milano, Dipartimento di Fisica, Milan, Italy
[d]ITMO University, Department of Physics, Saint Petersburg, Russia
[e]Ioffe Institute, Saint Petersburg, Russia
[f]Consiglio Nazionale delle Ricerche, Istituto di Fotonica e Nanotecnologie, Milan, Italy

Abstract. We predict theoretically a regime of photon-pair generation driven by the interplay of multiple bound states in the continuum resonances in nonlinear metasurfaces. This nondegenerate photon-pair generation is derived from the hyperbolic topology of the transverse phase matching and can enable orders-of-magnitude enhancement of the photon rate and spectral brightness, as compared to the degenerate regime. We show through comprehensive simulations that the entanglement of the photon pairs can be tuned by varying the pump polarization, which can underpin future advances and applications of ultracompact quantum light sources.

Keywords: optics; photonics; light; metasurface; spontaneous parametric down-conversion; entanglement.

Received Jun. 25, 2021; revised manuscript received Jul. 20, 2021; accepted for publication Aug. 9, 2021; published online Sep. 1, 2021.

[DOI: 10.1117/1.AP.3.5.055001]

1 Introduction

Metasurfaces (MSs) offer an ultracompact and versatile platform for enhancing nonlinear optical processes, including harmonic generation and frequency mixing.[1,2] To realize such nonlinear interactions in bulk crystals and waveguides, one requires extended propagation distances, but in MSs a strong enhancement of light–matter interactions can be achieved with subwavelength thicknesses through the excitation of high-quality factor optical resonances. Notably, this can be facilitated by designing Bound State in the Continuum (BIC) resonances,[3–7] which support a high confinement of the optical field within the nonlinear material.[8–10]

In addition to classical frequency mixing, nonlinear MSs can also, through Spontaneous Parametric Down-Conversion (SPDC), generate entangled photons with a strong degree of spatial coherence.[11] SPDC in carefully engineered MSs has the potential to drive fundamental advances in the field of ultracompact multi-photon sources[12] that operate at room temperature, which are suitable for integration in end-user devices with applications that include quantum imaging[13] and free-space communications.[14] Traditionally, SPDC is performed in bulk nonlinear crystals with dimensions up to centimeters in length, while integrated waveguides have enabled a reduction of the footprint to millimeter[15] and down to 100 μm length scales.[16] At the subwavelength scale, generation of photon pairs was reported experimentally from a single AlGaAs nanoresonator[17] and lithium niobate MSs,[18] and studies were also conducted on monolayers of MoS_2,[19] carbon nanotubes,[20] and directional emission from nanoresonators.[21]

Importantly, SPDC in ultrathin nonlinear layers[22–24] can give rise to strong spatial correlations and allow quantum state engineering without the constraints of longitudinal phase matching. It has been proposed that a so-called "accidental" BIC at the pump frequency can increase the photon rate at a single nanoresonator,[25] while a photonic crystal slab with a BIC resonance can enhance SPDC in a monolayer of WS_2,[26] although the theoretically estimated rate was still much lower than with conventional sources. There is now strong interest in new concepts and

*Address all correspondence to Matthew Parry, Matthew.Parry@anu.edu.au; Andrey A. Sukhorukov, Andrey.Sukhorukov@anu.edu.au

practical approaches for even stronger enhancement of the brightness of SPDC photon-pair generation in subwavelength scale structures.

In this theoretical paper, we present a general approach for orders-of-magnitude enhancement of the photon-pair generation rate and spectral brightness in nonlinear MSs. We reveal, for the first time, to the best of our knowledge, that nondegenerate SPDC efficiency can be dramatically increased when the signal and idler photons are supported by BIC resonances at different frequencies. We demonstrate how these features can be realized in practice by engineering the symmetry of the MS to deliver a projected spectral brightness five orders of magnitude higher than for an unpatterned film. Our results are fundamentally different from the recently demonstrated SPDC generation using linear MS-lenses that engineer the quantum state by focusing the pump at multiple spots in a bulk crystal.[27]

2 Principles and Methods

We demonstrate that a MS with reduced global rotational symmetry allows much greater flexibility in tailoring the dispersion from several BICs, in which the signal and idler photons are generated. Consequently, we can control the form of the transverse phase matching for SPDC according to the energy and momentum conservation, as illustrated in Fig. 1(a):

$$\mathbf{k}_{p,\perp} = \mathbf{k}_{s,\perp} + \mathbf{k}_{i,\perp}, \tag{1}$$

$$\omega_p(\mathbf{k}_{p,\perp}) = \omega_s(\mathbf{k}_{s,\perp}) + \omega_i(\mathbf{k}_{i,\perp}), \tag{2}$$

where the indices refer to pump (p), signal (s), and idler (i) photons with the corresponding frequencies ω. The wave-vectors $\mathbf{k}$ define the propagation directions in free space, and $\perp$ indicates the transverse components in the plane of the MS. We note that the photon polarization weakly affects phase matching (see Sec. S6 in the Supplementary Material).

We focus on a MS with D_{2h} symmetry and outline other possibilities in Sec. S2 in the Supplementary Material. According to our concept, we designed a MS composed of a square array of cylinders with two holes, or ghost oligomers, inserted to remove the 90-deg rotational symmetry [Fig. 1(b)]. This structure supports multiple extended photonic-crystal-like BICs,[3] where the field localization arises from a mismatch between the symmetry of the collective modes and the available radiation channels.

We consider resonators made of $Al_{0.18}Ga_{0.82}As$, which possess strong quadratic nonlinearity and can be manufactured with established procedures. We chose a (111) crystal orientation, as it provides the best off-BIC conversion efficiency in the normal propagation direction (see Sec. S3 in the Supplementary Material) and hence gives a better measure of the enhancement due to the BIC. In our modeling, we have omitted a substrate to focus on the generic features (see Sec. S1 in the Supplementary Material for details on the simulation methods). Adding a substrate will convert the BICs to quasi-BICs, due to the up/down asymmetry introduced. But as we discuss in the following, the photon generation is associated with quasi-BICs formed by off-normal angles, thus confirming that the ideal BICs with formally infinite quality factors are not required.

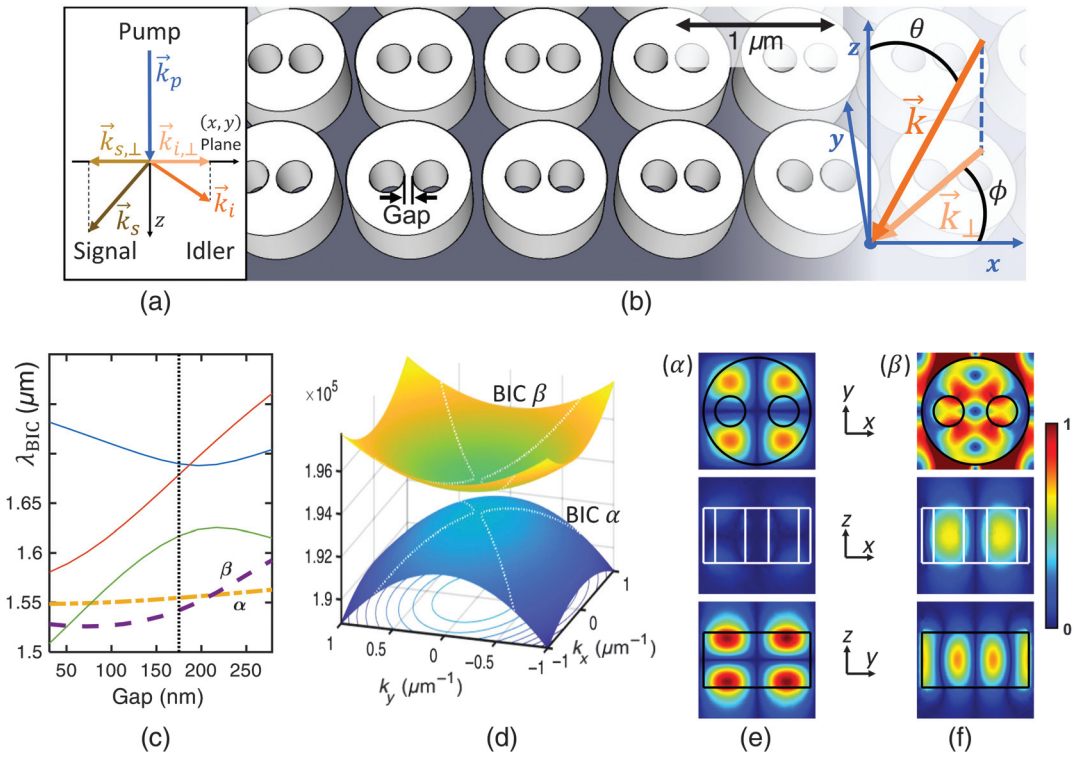

Fig. 1 The MS and its modes. (a) Diagram of transverse phase matching. (b) MS design and the coordinate axes: θ is the polar and ϕ the azimuthal angle. (c) BIC wavelengths versus the gap between the two holes. (d) The dispersion for two quasi-BICs: (α) lower and (β) upper surfaces. Dotted white lines: two-BIC phase matching for $\lambda_p = 774.22$ nm. (e), (f) Fields $|\mathbf{E}|$ of the two BICs.

We therefore conclude that a strong enhancement will still be achieved when a substrate is present. Our general approach can also be applied to MSs made of different nonlinear materials, including lithium niobate, where efficient classical frequency conversion has been demonstrated.[28–30]

An important feature of BICs is that changes in the dimensions of the meta-atoms will not destroy a photonic-crystal like BIC so long as the relevant symmetry is maintained. This enables simultaneous tuning of the resonant frequencies for several BICs by adjusting the design parameters, such as the separation between the hole pairs, as shown in Fig. 1(c). By shifting the position of the holes, the proportion of the electric field within these two low refractive index regions changes, which in turn changes the energy of the modes. The way in which each mode is affected depends on the profile of the mode over the region through which the holes move. Similar configurability is found with the other dimensions of the meta-atoms. This tunability offers an important advantage with SPDC generation when compared to using so-called accidental BICs[31] in individual nanoresonators, which only appear at very specific resonator dimensions.

The dispersion of the two BICs studied in this paper is shown in Fig. 1(d), which, importantly, have opposite dispersion. Their mode profiles are shown in Figs. 1(e) and 1(f), where the fields are normalized to the peak value inside the resonator for each BIC. They are also marked α and β in Fig. 1(c), where the dotted line shows the value of the gap used in the two-BIC study. The single BIC study uses BIC α [Fig. 1(e)] with a gap of 52 nm, which gives a good separation from the other BICs.

3 Results

3.1 Single BIC

As a first study, we present an analysis of SPDC with the signal and idler photons being generated at a single BIC. We calculated the SPDC generation rate via the quantum-classical correspondence between SPDC and sum frequency generation (SFG),[11,17,32,33] which is exact in the absence of other nonlinear effects. We performed full SFG numerical simulations and used these results to predict the efficiency of quantum photon-pair generation through SPDC:

$$\Xi_{\mathrm{SPDC}} = \frac{1}{(2\pi)^3}\frac{\lambda_p^2}{\lambda_s^{\mathrm{BIC}}\lambda_i^{\mathrm{BIC}}}\frac{\Phi_{\mathrm{SFG}}}{\Phi_s\Phi_i}, \tag{3}$$

where Φ_{SFG} is the zeroth order far-field SFG intensity, and Φ_s and Φ_i are the incident signal and idler intensities. For SPDC calculations, we take the small angle approximation, where in the far-field the z component is zero, so the $|H\rangle$ and $|V\rangle$ notations indicate the polarization primarily along the x and y axes, respectively. The solid line in Fig. 2(a) shows the results of such modeling.

We then confirmed that the SPDC generation is approximately proportional to the product of the maximum intensity of the signal and idler electric fields inside the resonator. We present a typical dependence of this quantity near a BIC resonance, obtained from linear simulations, with the dashed line in Fig. 2(a), where there is a slightly off-normal signal and idler ($\theta_s = 0.2$ deg), and the pump wavelength is $\lambda_p = 775$ nm. We can see that the shapes of solid and dashed lines match closely. This is a physically important observation, as it means

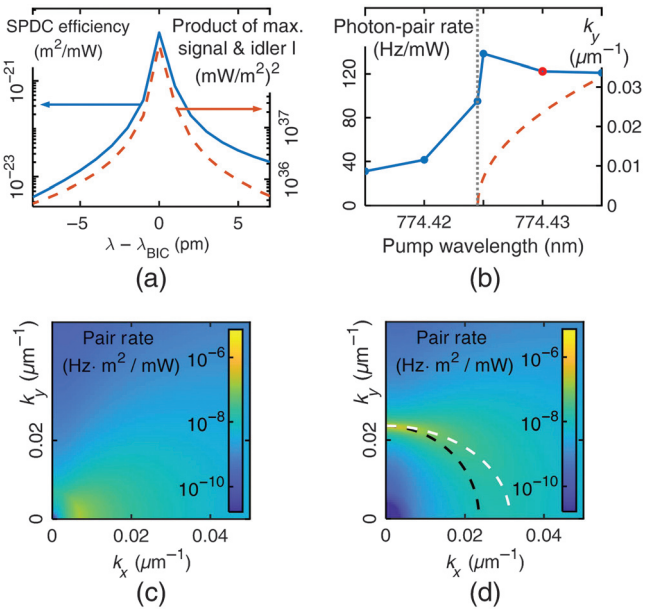

Fig. 2 SPDC at a single BIC. (a) Solid line: the generation rate for a horizontally polarized, normally incident pump, $|HH\rangle$ signal and idler state, $\phi = 79$ deg and $\theta_s = 0.2$ deg for the signal, opposite angle for the idler. Dashed line: the product of the maximum intensity inside the resonator of the signal and idler fields. (b) Solid line: generation rate versus the pump wavelength. The red dot marks the wavelength used in (d) and Fig. 4. Dashed: k_y at phase matching when $k_x = 0$. (c), (d) Generation rate in k-space for (c) phase matching at the Γ point and (d) for $\lambda_p = 774.43$ nm. White dashed line: phase matching condition; black dashed line: the path of constant θ_s in Fig. 4(a).

that the designed MS optimally translates the BIC enhancement of the signal and idler to a corresponding increase of SPDC.

We conducted studies of the intensity enhancement for different angles of θ_s and ϕ_s. The simulated intensities are fitted to a Lorentzian function $L(\omega, \mathbf{k})$ (see Sec. S5 in the Supplementary Material), and, from this fitted function, we calculate

$$\Xi_{\mathrm{SPDC}} = \frac{1}{(2\pi)^3}\frac{\lambda_p^2}{\lambda_s^{\mathrm{BIC}}\lambda_i^{\mathrm{BIC}}}\sum_{\substack{|HH\rangle,|HV\rangle,\\|VH\rangle,|VV\rangle}}\Xi_0 L(\omega_s, \mathbf{k_s})L(\omega_p - \omega_s, \mathbf{k}_p - \mathbf{k_s}), \tag{4}$$

where Ξ_0 is the ratio of the SFG zeroth diffraction order far-field intensity to the product of the maximum signal and idler intensities inside the resonator (see Sec. S4 in the Supplementary Material). The sum is taken over all polarization combinations of horizontal ($|H\rangle$) and vertical ($|V\rangle$) for the signal and idler, which forms the polarization basis for our wavefunction. The total photon pair generation rate across all angles and wavelengths can then be calculated via

$$\frac{1}{A_{\mathrm{tot}}\Phi_p}\frac{\mathrm{d}N_{\mathrm{pair}}}{\mathrm{d}t} = \iiint \Xi_{\mathrm{SPDC}}\mathrm{d}\omega_s\,\mathrm{d}k_{s,x}\,\mathrm{d}k_{s,y}, \tag{5}$$

where A_{tot} is the total sample area, and Φ_p is the incident pump intensity.

If we only integrate Eq. (5) over frequency, then we will obtain the pair-rate as a function of the signal wavevector, as seen in Figs. 2(c) and 2(d). Figure 2(c) has a pump wavelength at which the transverse phase matching condition occurs at the Γ point, and Fig. 2(d) has $\lambda_p = 774.43$ nm, which was chosen for illustrative purposes. Note that the pair-rate falls off near the Γ point, as symmetry protected BICs have singularities at the Γ point. We therefore only see enhancement in the off-Γ, quasi-BIC regime. In Fig. 2(d), the dashed white line shows the angle in k-space at which the transverse phase matching condition occurs, which matches the peak in generation as expected.

By then integrating over k-space, we obtain the total photon-pair generation rate as a function of the pump wavelength, as shown with a solid line in Fig. 2(b). Notably, the peak does not occur at the Γ point but just beyond it, as can be seen by comparing this plot with the dashed line showing the value of k_y at the transverse phase matching condition when $k_x = 0$. This, again, is due to the singularity at the Γ point. We calculate the theoretical peak brightness of this quasi-BIC to be $110\ \mathrm{Hz} \cdot \mathrm{mW}^{-1} \cdot \mathrm{nm}^{-1}$ over a 1.3-nm bandwidth, which is 2×10^3 that of simulations of an unpatterned nonlinear film.

3.2 Two BICs

Next, we studied the case where the signal and idler are generated at two different BICs. The most distinguishing feature here is the occurrence of hyperbolic transverse phase matching, as shown in Fig. 3(a), calculated according to the right-hand side of Eq. (2) for the normally incident pump with $\mathbf{k}_{p,\perp} = 0$. The condition for the pump wavelength of $\lambda_p = 774.22$ nm is shown by the dotted white line in Figs. 1(d), 3(a), and 3(d).

For the two-BIC case, in Fig. 3(c), we show the angular dependence in k-space of the photon-pair generation when transverse phase matching occurs at the Γ point, and, in Fig. 3(d), the case in which $\lambda_p = 774.22$ nm. As before, there is a peak in generation at the transverse phase matching condition (dashed white line). In Fig. 3(b), we see that the photon-pair generation rate is almost two orders of magnitude higher than for the single BIC case in Fig. 2(b). A factor of 6 of the enhancement can be attributed to different mode profiles and their overlap (see Sec. S4 in the Supplementary Material). Importantly, an order-of-magnitude increase is due to hyperbolic phase matching, whereby SPDC enhancement occurs for a much broader range of transverse photon wavevectors, in contrast to the single BIC case with elliptical phase matching only allowing a small range of wavevectors close to the Γ point. We calculated the theoretical peak brightness to be $4900\ \mathrm{Hz} \cdot \mathrm{mW}^{-1} \cdot \mathrm{nm}^{-1}$ over a 1.2-nm bandwidth, which is 10^5 that of simulations for an unpatterned nonlinear film. Such predicted brightness enhancement is also much stronger than for MSs based on Mie-like resonances.[18]

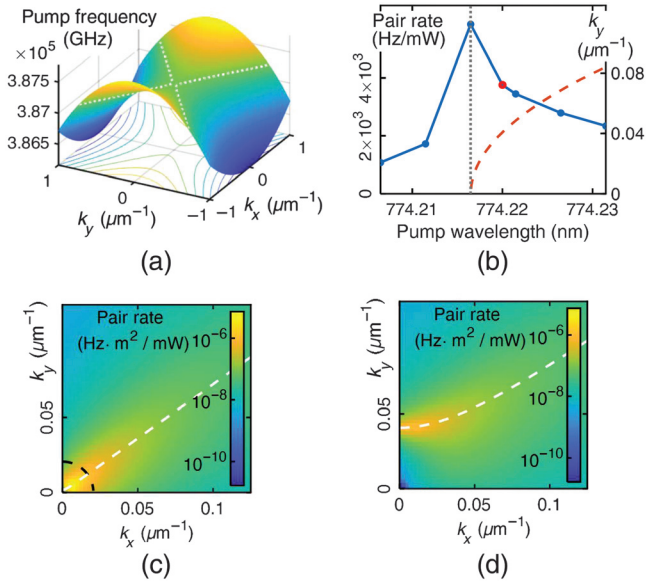

Fig. 3 Nondegenerate signal and idler at different BICs. (a) Transverse phase matching condition according to Eq. (2). The dotted white line corresponds to $\lambda_p = 774.22$ nm. (b) Solid line: generation rate versus the pump wavelength. The red circle is the integration of (d). Dashed line: k_y at transverse phase matching when $k_x = 0$. (c), (d) Generation rate in k-space at (c) phase matching at the Γ point ($\lambda_p = 774.2165$ nm) and (d) $\lambda_p = 774.22$ nm. White dashed line: phase matching condition; black dashed line: the path of constant θ_s in Fig. 4(c).

3.3 Entanglement

We determined the polarization entanglement of the generated signal and idler by performing a Schmidt decomposition (see Sec. S7 in the Supplementary Material), where the Schmidt number $K = 1$ indicates no entanglement and $K = 2$ maximum entanglement. In Fig. 4(a), we show that for the single BIC case the entanglement peaks at $K = 2$ when the azimuthal angle of the signal-photon emission is $\phi_s = 77$ deg, and the pump is horizontally polarized. The maximally entangled signal and

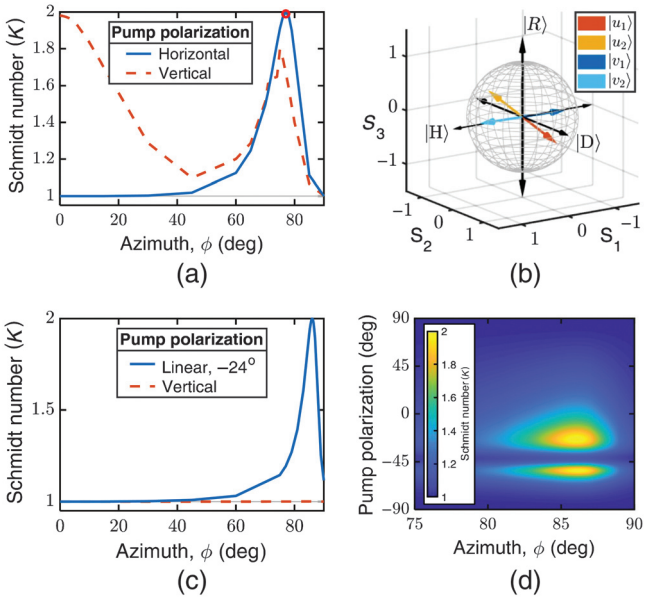

Fig. 4 Entanglement of the signal and idler photons generated from: (a), (b) a single BIC with $\lambda_p = 774.43$ nm; (c), (d) two different BICs with $\lambda_p = 774.2165$ nm. (a), (c) Schmidt number versus the photon angle. (b) Schmidt decomposition of the wavefunction plotted on the Poincaré sphere for the red dot in (a). (d) Schmidt number versus the pump polarization and photon angle.

idler pair states $\{|u_1\rangle, |v_1\rangle\}$ or $\{|u_2\rangle, |v_2\rangle\}$ are visualized in Fig. 4(b). For the two-BIC case, we can switch from full to no entanglement by changing the linear polarization of the pump [see Figs. 4(c) and 4(d)].

4 Discussion

The two elliptic paraboloids in Fig. 1(d) can only sum to a hyperbolic paraboloid because the MS lacks $\pi/2$ in-plane rotational symmetry. The D_{2h} symmetry of the MS means that the BICs must have an elliptic paraboloid dispersion near the ω point, as that matches the rotation and mirror symmetries of the MS. In our case, k_x and k_y are the major and minor axes, but a set of axes can always be chosen such that the dispersion is of the form

$$\omega(\mathbf{k}_\perp) = \zeta\left(\frac{k_x^2}{a^2} + \frac{k_y^2}{b^2}\right) + \omega_0, \tag{6}$$

where $\zeta = \pm 1$. The transverse phase matching condition, for a pump with normal incidence, is thus given by

$$\begin{aligned}\omega_p(\mathbf{k}_{p,\perp} = 0) &= \omega_s(\mathbf{k}_{s,\perp}) + \omega_i(\mathbf{k}_{i,\perp} = -\mathbf{k}_{s,\perp}) \\ &= k_{s,x}^2\left(\frac{\zeta_s}{a_s^2} + \frac{\zeta_i}{a_i^2}\right) + k_{s,y}^2\left(\frac{\zeta_s}{b_s^2} + \frac{\zeta_i}{b_i^2}\right) + \omega_{s,0} + \omega_{i,0} \\ &= \zeta_x \frac{k_{s,x}^2}{a_p^2} + \zeta_y \frac{k_{s,y}^2}{b_p^2} + \omega_{p,0},\end{aligned} \tag{7}$$

which can be either an elliptic or hyperbolic paraboloid, with the latter enabling enhanced photon-pair generation, as discussed above. In contrast, for an MS with D_{4h} symmetry (such as a slab with a square array of single holes), $\zeta_x \equiv \zeta_y$ and $a_p \equiv b_p$, which excludes a hyperbolic type of transverse phase matching.

We note that the symmetry properties enabling hyperbolic transverse phase matching will also hold when taking into account a MS substrate, as the presence of a substrate will convert the BICs at the Γ point into quasi-BICs, and the dominant emission of the photon pairs occurs in the off Γ (off-normal) direction in the quasi-BIC regime in any case, as shown in Figs. 2 and 3. These results suggest that strong SPDC enhancement will still persist in the presence of a substrate.

The influence of experimental imperfections on the other hand depends on their type. If the dimensions of the nanostructures, for example, the hole sizes, are varied equally in the whole MS, then the BIC states will remain, and the SPDC enhancement will be preserved, usually at slightly shifted wavelengths similar to the dependencies shown in Fig. 1(c). On the other hand, the random deviations in individual unit cells that effectively break the periodicity could lead to significant deterioration of the quality-factors, since the extended BIC states are based on resonances across multiple nanoresonators. Accordingly, for the best SPDC enhancement, it would be most important to maintain consistent periodic nanopatterning over the whole spatial extent of the MS. Additionally, the MS dimensions should be sufficiently large, with tens or hundreds of periods in each spatial direction, to avoid limitations on the resonance Q factor.[6,34] These conditions can be achieved with the state-of-the-art nanofabrication facilities. For example, ultrahigh Q factors of over 10,000 in dielectric MSs were reported for extended BICs.[6]

5 Conclusion

We have developed a method of enhanced photon-pair generation via symmetry protected BICs in nonlinear MSs, which are designed to realize a hyperbolic transverse phase matching condition. In terms of the brightness of the photon pair-generation, our nanoscale platform provides five orders of magnitude improvement over unpatterned films. Additional benefits are the tunability of the photon wavelengths and the degree of polarization entanglement. We anticipate that these predictions can stimulate significant experimental advances in miniaturized quantum light sources based on ultrathin nonlinear MSs for fundamental research and applications.

Acknowledgments

The authors would like to thank Jihua Zhang for the useful discussions and comments. We would like to acknowledge the support by the Australian Research Council (Nos. DP190101559, CE200100010, and FT170100331). A. M. and G. D. V. would like to acknowledge the support of the European Union Horizon 2020 Research and Innovation Programme through the METAFAST project (Grant No. 899673). The authors declare no conflicts of interest.

Code, Data, and Materials Availability

The COMSOL simulations were run using a specially developed code, which is made available at https://github.com/mettw/COMSOLd.

References

1. G. Li, S. Zhang, and T. Zentgraf, "Nonlinear photonic metasurfaces," *Nat. Rev. Mater.* **2**(5), 17010 (2017).
2. C. De Angelis, G. Leo, and D. N. Neshev, *Nonlinear Meta-Optics*, CRC Press, London (2020).
3. C. W. Hsu et al., "Bound states in the continuum," *Nat. Rev. Mater.* **1**(9), 16048 (2016).
4. M. V. Rybin et al., "High-Q supercavity modes in subwavelength dielectric resonators," *Phys. Rev. Lett.* **119**(24), 243901 (2017).
5. K. Koshelev et al., "Asymmetric metasurfaces with high-Q resonances governed by bound states in the continuum," *Phys. Rev. Lett.* **121**(19), 193903 (2018).
6. Z. J. Liu et al., "High-Q quasibound states in the continuum for nonlinear metasurfaces," *Phys. Rev. Lett.* **123**(25), 253901 (2019).
7. K. Koshelev et al., "Subwavelength dielectric resonators for nonlinear nanophotonics," *Science* **367**(6475), 288–292 (2020).
8. P. P. Vabishchevich et al., "Enhanced second-harmonic generation using broken symmetry III-V semiconductor Fano metasurfaces," *ACS Photonics* **5**(5), 1685–1690 (2018).
9. L. Carletti et al., "Second harmonic generation in monolithic lithium niobate metasurfaces," *Opt. Express* **27**(23), 33391–33398 (2019).
10. Z. Huang et al., "Highly efficient second harmonic generation of thin film lithium niobate nanograting near bound states in the continuum," *Nanotechnology* **32**(32), 325207 (2021).
11. A. N. Poddubny, D. N. Neshev, and A. A. Sukhorukov, "Quantum nonlinear metasurfaces," in *Nonlinear Meta-Optics*, C. De Angelis, G. Leo, and D. N. Neshev, Eds., pp. 147–180, CRC Press, London (2020).
12. A. S. Solntsev, G. S. Agarwal, and Y. S. Kivshar, "Metasurfaces for quantum photonics," *Nat. Photonics* **15**(5), 327–336 (2021).
13. M. G. Basset et al., "Perspectives for applications of quantum imaging," *Laser Photonics Rev.* **13**(10), 1900097 (2019).

14. F. Steinlechner et al., "Distribution of high-dimensional entanglement via an intra-city free-space link," *Nat. Commun.* **8**(1), 15971 (2017).
15. A. Orieux et al., "Direct Bell states generation on a III-V semiconductor chip at room temperature," *Phys. Rev. Lett.* **110**(16), 160502 (2013).
16. M. J. Collins et al., "Integrated spatial multiplexing of heralded single-photon sources," *Nat. Commun.* **4**(1), 2582 (2013).
17. G. Marino et al., "Spontaneous photon-pair generation from a dielectric nanoantenna," *Optica* **6**(11), 1416–1422 (2019).
18. T. Santiago-Cruz et al., "Photon pairs from resonant metasurfaces," *Nano Lett.* **21**(10), 4423–4429 (2021).
19. H. D. Saleh et al., "Towards spontaneous parametric down conversion from monolayer MoS_2," *Sci. Rep.* **8**(1), 3862 (2018).
20. K. F. Lee et al., "Photon-pair generation with a 100 nm thick carbon nanotube film," *Adv. Mater.* **29**(24), 1605978 (2017).
21. A. Nikolaeva et al., "Directional emission of down-converted photons from a dielectric nanoresonator," *Phys. Rev. A* **103**(4), 043703 (2021).
22. C. Okoth et al., "Microscale generation of entangled photons without momentum conservation," *Phys. Rev. Lett.* **123**(26), 263602 (2019).
23. C. Okoth et al., "Idealized Einstein–Podolsky–Rosen states from non-phase-matched parametric down-conversion," *Phys. Rev. A* **101**(1), 011801(R) (2020).
24. T. Santiago-Cruz et al., "Entangled photons from subwavelength nonlinear films," *Opt. Lett.* **46**(3), 653–656 (2021).
25. A. N. Poddubny and D. A. Smirnova, "Nonlinear generation of quantum-entangled photons from high-Q states in dielectric nanoparticles," arXiv:1808.04811 (2018).
26. T. C. Wang et al., "Improved generation of correlated photon pairs from monolayer WS_2 based on bound states in the continuum," *Photonics Res.* **7**(3), 341–350 (2019).
27. L. Li et al., "Metalens-array-based high-dimensional and multiphoton quantum source," *Science* **368**(6498), 1487–1490 (2020).
28. J. Ma et al., "Resonantly tunable second harmonic generation from lithium niobate metasurfaces," arXiv:2002.06594 (2020).
29. Z. J. Huang et al., "Fano resonance on nanostructured lithium niobate for highly efficient and tunable second harmonic generation," *Nanomaterials (Basel)* **9**(1), 69 (2019).
30. A. Fedotova et al., "Second-harmonic generation in resonant nonlinear metasurfaces based on lithium niobate," *Nano Lett.* **20**(12), 8608–8614 (2020).
31. L. Carletti et al., "Giant nonlinear response at the nanoscale driven by bound states in the continuum," *Phys. Rev. Lett.* **121**(3), 033903 (2018).
32. A. N. Poddubny et al., "Generation of photon-plasmon quantum states in nonlinear hyperbolic metamaterials," *Phys. Rev. Lett.* **117**(12), 123901 (2016).
33. F. Lenzini et al., "Direct characterization of a nonlinear photonic circuit's wave function with laser light," *Light Sci. Appl.* **7**(1), 17143 (2018).
34. M. S. Bin-Alam et al., "Ultra-high-Q resonances in plasmonic metasurfaces," *Nat. Commun.* **12**(1), 974 (2021).
35. L. Carletti et al., "Controlling second-harmonic generation at the nanoscale with monolithic AlGaAs-on-AlOx antennas," *Nanotechnology* **28**(11), 114005 (2017).
36. D. Schattschneider, "Plane symmetry groups—their recognition and notation," *Am. Math. Monthly* **85**(6), 439–450 (1978).
37. J. D. Sautter et al., "Tailoring second-harmonic emission from (111)-GaAs nanoantennas," *Nano Lett.* **19**(6), 3905–3911 (2019).
38. S. Buckley et al., "Second-harmonic generation in GaAs photonic crystal cavities in (111)B and (001) crystal orientations," *ACS Photonics* **1**(6), 516–523 (2014).
39. Y. J. Lu and Z. Y. Ou, "Optical parametric oscillator far below threshold: experiment versus theory," *Phys. Rev. A* **62**(3), 033804 (2000).
40. M. V. Fedorov and N. I. Miklin, "Schmidt modes and entanglement," *Contemp. Phys.* **55**(2), 94–109 (2014).
41. I. Lankham, B. Nachtergaele, and A. Schilling, *Linear Algebra as an Introduction to Abstract Mathematics*, World Scientific, Singapore (2016).
42. P. Kaye, R. Laflamme, and M. Mosca, *An Introduction to Quantum Computing*, Oxford University Press, Oxford (2007).

Matthew Parry received his bachelor's degree from the University of New South Wales, Sydney, Australia. He is a PhD student at the Australian National University (ANU). His research interests are in metasurfaces, especially with respect to quantum applications. He is a member of SPIE.

Andrea Mazzanti received his MSc degree in engineering physics from Politecnico di Milano, Milan, Italy, in 2017 and his PhD in 2021. His research interests include the design and modeling of optical metastructures for a variety of nanophotonic applications, such as nonlinear frequency generation, plasmonic nanoheater aggregates assisted drug delivery, and all-optically controllable dielectric metasurfaces.

Alexander Poddubny received his PhD from Ioffe Institute, St. Petersburg, Russia, in 2008 and became a professor of the Russian Academy of Sciences in 2018. He is an Australian future fellow at the ANU and a senior researcher at the Ioffe Institute. His current research interests include quantum optics, many-body physics, and optomechanics.

Giuseppe Della Valle is a professor in the Physics Department of the Politecnico di Milano, where he teaches courses of general physics, nano-optics, and plasmonics. His research activity is devoted to both theoretical and experimental research in physics and optics, with particular interest to the development of innovative photonic structures at the micro- and nanoscale for the generation and coherent control of light.

Dragomir N. Neshev is a professor in physics at the ANU and the director of the Australian Research Council Centre of Excellence for Transformative Meta-Optical Systems (TMOS). He has worked in the field of optics at several research centers and joined the ANU in 2002. His activities span over several branches of optics, including periodic photonic structures, singular optics, plasmonics, and optical metasurfaces.

Andrey A. Sukhorukov is a professor at the Research School of Physics of the ANU. He leads a research group on nonlinear and quantum photonics, targeting the fundamental aspects of miniaturization of optical elements down to micro- and nanoscale. In 2015, he was elected a fellow of The Optical Society for contributions to nonlinear and quantum integrated photonics, including frequency conversion and broadband light manipulation in waveguide circuits and metamaterials.